Density functional theory study of mercury adsorption on metal surfaces

Janice A. Steckel[*]

National Energy Technology Laboratory, United States Department of Energy, P.O. Box 10940, Pittsburgh, Pennsylvania 15236, USA
and Parsons Project Services, Inc., South Park, Pennsylvania 15129, USA

Density functional theory (DFT) calculations are used to characterize the interaction of mercury with copper, nickel, palladium, platinum, silver, and gold surfaces. Mercury binds relatively strongly to all the metal surfaces studied, with binding energies up to ~1 eV for Pt and Pd. DFT calculations underestimate the energy of adsorption with respect to available experimental data. Plane-wave DFT results using the local density approximation and the Perdew-Wang 1991 and Perdew-Burke-Ernzerhof parametrizations of the generalized gradient approximation indicate that binding of mercury at hollow sites is preferred over binding at top or bridge sites. The interaction with mercury in order of increasing reactivity over the six metals studied is Ag < Au < Cu < Ni < Pt < Pd. Binding is stronger on the (001) faces of the metal surfaces, where mercury is situated in fourfold hollow sites as opposed to the threefold hollow sites on (111) faces. In general, mercury adsorption leads to decreases in the work function; adsorbate-induced work function changes are particularly dramatic on Pt.

I. INTRODUCTION

Many natural materials such as coal and oil contain small amounts of mercury. When these materials are used on a large scale, such as in the burning of fuel to produce electricity, mercury is released into the atmosphere. Current releases of mercury into the atmosphere as a result of human activity are estimated to be ~2400 tons per year.[1] Mercury contamination of the atmosphere and the bioaccumulation of mercury in fish have led to policy changes in the United States including a two-phase cap on mercury emissions from coal-fired power plants. Emission reductions for the first phase are expected to be achieved as a cobenefit of technologies that control other air pollutants, but it is expected that the second, lower cap on emissions will require the development of dedicated mercury-control technologies.[2]

About 25% of the electricity produced from coal in the United States comes from plants that are equipped with wet flue gas desulfurization (WFGD) units for the removal of sulfur (responsible for acid rain). The WFGD units are capable of removing ~90% of oxidized mercury from the flue, but they do not remove mercury in elemental form, and therefore the overall efficiency of mercury removal across a WFGD unit will vary according to the speciation of the mercury that enters the device.[3] In order to ensure the efficiency of mercury removal via WFGD units, there is a need for effective and regenerable mercury oxidation catalyst materials, and noble metals such as copper, silver, gold, and palladium are being investigated for this application.[4–6]

Noble metals including platinum, gold, palladium, and copper have been investigated for incorporation in novel mercury removal sorbents, both for conventional coal-fired power plants and in the context (i.e., different temperature and pressure) of new integrated gasification combined-cycle (IGCC) power generation plants.[7,8]

Despite the interest in using metals in mercury removal, very little research has been carried out to determine basic information about the binding of mercury to metal surfaces.

In this paper, density functional theory (DFT) calculations are used to characterize the bonding of mercury to the surface of a series of metals. This project represents a survey of the adsorption interaction of mercury with the ideal metal surfaces as calculated by plane-wave DFT methods. In addition to providing fundamental information about the interaction of mercury with specific metal surfaces, comparisons are made between metals and between different overlayer patterns.

II. PREVIOUS WORK

Theoretical calculations on mercury can be quite challenging as bonding in mercury varies from primarily van der Waals in the dimer to covalent in small clusters to metallic in large clusters and in the bulk.[9,10] Relativistic effects play an important role in the degree of $6s$-$6p$ and $6s$-$5d$ hybridization in the electronic structure and the magnitude of metallic bonding in mercury.[11,12] All-electron calculations on mercury are computationally expensive, and much effort has been devoted to the development of effective core potentials (ECPs) as well as balanced basis sets for use in mercury calculations.[13–18] A sophisticated description of electron correlation and treatment of relativistic effects including spin-orbit coupling are desirable for highly accurate results.[19–21] The use of ECPs generated from relativistic all-electron calculations can not only reduce the number of electrons that must be treated explicitly, but contributions of the most important relativistic operators are transferred to the pseudopotential.[14] Much high-quality *ab initio* work on small mercury compounds (including the mercury halides) has been performed using wave-function-based methods and small-core ECPs.[22–25] For small molecules, these methods are state of the art, but there is also a push to find ways to perform simulations on larger mercury clusters as well as mercury adsorption to the surfaces of solids.[9,10,21,26] Calculations carried out by Gaston *et al.* on mercury dimers, mercury clusters, and bulk mercury have revealed inaccuracies

in many of the common theoretical tools in use for larger clusters or solids.[9,20,21] Despite its shortcomings, DFT remains an important tool for the description of mercury and compounds or materials interacting with mercury, quite simply because more accurate methods cannot currently be applied to very large clusters or with the use of periodic boundary conditions. The use of a relativistic formulation of DFT in mercury bonding is desirable but it is difficult to treat models larger than ~30 heavy atoms. Using four-component relativistic DFT with a series of embedded-cluster models of various sizes, Sarpe-Tudoran and co-workers calculated binding energies for Hg to Au(001) of −1.01, −1.52, and −0.84 eV for top, bridge, and hollow sites, respectively.[27] The authors point out that the binding energies were not converged with respect to cluster size due to the high cost of the theoretical method.

There have been a number of experimental studies of mercury on metal surfaces.[28–35] On the (001) surface of Ag, where the mesh dimension is close to the Hg-Hg distance in α-Hg (3.005 Å),[21] initial growth of Hg layers has been shown to be pseudomorphic and a $c(1 \times 1)$ low-energy electron diffraction (LEED) pattern has been observed.[29,32,34] The heat of desorption for the $c(1 \times 1)$ phase of Hg on Ag(001) was reported to be 0.63 eV.[32] The lattice dimensions of Cu and Ni are smaller, and the $c(1 \times 1)$ phase has not been observed. The heats of desorption for the $c(2 \times 2)$ and $c(4 \times 4)$ phases of Hg on Cu(001) was reported to be 0.74 and 0.70 eV, respectively.[32]

Several experimental studies were carried out on mercury adsorption on Ni(001) and Ni(111) surfaces by Jones and collaborators.[28,30,31,33] Jones and Tong proposed a mobile two-dimensional lattice gas model for mercury adsorption on Ni(001) at low coverages, followed by a transition to an immobile $c(2 \times 2)$ adsorption as coverage increases and to an incommensurate overlayer at higher coverages. They found strong chemisorption of mercury on Ni(001), with an associated $c(2 \times 2)$ LEED pattern (except for the highest coverages, for which the LEED pattern was more complicated). They measured a heat of adsorption at zero coverage of 1.19 ± 0.16 eV; as coverage increased, so did the heat of adsorption, peaking at 1.71 ± 0.16 eV and then dropping to 1.04 ± 0.16 eV.

Using standing x-ray wave-field absorption experiments, Prince *et al.* studied the $c(2 \times 2)$-Hg/Ni(001) overlayer.[30] They measured a Hg to Ni lattice plane spacing of 0.6 ± 0.1 Å, which is consistent with with Hg adsorption at bridge sites. Subsequently, Poulsen *et al.* performed transmission channeling studies and concluded that adsorption of Hg on Ni(001) below 0.5 monolayer (ML) occurs at the fourfold hollow sites at a height of 2.25 ± 0.10 Å.[34] On the Ni(111) surface, Singh and Jones measured a heat of adsorption of 1.14 ± 0.41 eV at zero coverage, 2.07 ± 0.41 eV for the $(\sqrt{3} \times \sqrt{3})R30°$-Hg/Ni(111) 0.333 ML overlayer and 0.83 ± 0.41 eV for the $p(2 \times 2)$-Hg/Ni(111) 0.5 ML overlayer.[31] The increase of the heat of adsorption of mercury on the Ni(111) surface as a function of increasing coverage is similar to that which was found on the Ni(001) surface. Mercury overlayers have also attracted the interest of various scientists in the context of the nonmetal to metal

transition occurring in mercury overlayers and thin films.[36,37]

Recently, Soverna and colleagues used thermochromatic methods to evaluate the adsorption enthalpies of mercury on noble metal surfaces.[35] They found that mercury interacted with the following metals with increasing strength: Ag < Ni < Au < Pd < Pt. The binding energies obtained were Ag, $−0.91 \pm 0.03$ eV; Ni, $−0.92 \pm 0.03$ eV; Au, $−1.01 \pm 0.03$ eV; Pd, $−1.44 \pm 0.04$ eV; and Pt, $−1.49 \pm 0.05$ eV.

III. METHODS

As discussed above, there are shortcomings that accompany the use of DFT for the calculation of mercury adsorption on metals, but plane-wave DFT remains the practical compromise between accuracy and computational demand for studies of adsorption on metal surfaces in which periodic boundary conditions or a very large model are absolutely necessary. The DFT calculations were performed with the Vienna *ab initio* simulation package (VASP),[38,39] and made use of the projector augmented wave (PAW) method of Blöchl.[40,41] The Perdew-Zunger parametrization of the local exchange-correlation functional according to the quantum Monte Carlo simulations of Ceperley and Alder was used [hereafter denoted as the local density approximation (LDA)].[42,43] Two versions of nonlocal corrections in the form of the generalized gradient approximation were also used; that of Perdew and Wang[44,45] is denoted PW91 and that of Perdew, Burke, and Ernzerhof[46] is denoted PBE.

To accelerate the convergence, a generalized Gaussian smearing according to Methfessel and Paxton was adopted with order 1 and a width of 0.05 eV.[47] The size of the smearing width was chosen in order to keep the difference between the calculated free energy and total energy smaller than 1 meV/atom. All total energies have been extrapolated to $k_B T = 0$ eV.

A. Methods: Bulk properties

Calculations were carried out on bulk models of Ag, Au, Cu, Ni, Pd, and Pt in order to compare calculated bulk properties with experimentally measured properties for the density functionals mentioned above (LDA, PW91, and PBE). The volume versus energy data were fit to a Birch-Murnaghan equation of state to calculate the equilibrium lattice constant, bulk modulus, and cohesive energy. The details are presented as supplementary information (see Ref. 48).

As in previous reports,[49] DFT methods predict lattice constants in very good agreement with experimentally measured values. The functional that provided the best overall results for the six metals was the PBE functional, and therefore the PBE functional was used in most of the subsequent calculations.

B. Methods: Slab models

Interactions of mercury with the (001) and (111) surfaces of Ag, Au, Cu, Ni, Pd, and Pt have been studied with plane-wave DFT calculations on slab models. The metal surfaces have been represented with asymmetric four-layer slab models with atoms in the two lower layers fixed at ideal bulk

positions. Atoms in the top two layers of the slab, as well as the Hg overlayer, were allowed to relax. Slabs were separated by vacuum layers of ~10 Å or more. Atomic relaxations were carried out by minimization of the Hellmann-Feynman forces via a conjugate gradients algorithm. Relaxations were stopped when the absolute values of calculated forces on unfixed atoms were less than 1.0×10^{-5} eV/Å.

Optimization of the geometry for each supercell was followed by a separate single-point energy calculation at the converged geometry with fast Fourier transform (FFT) meshes sufficiently large to include all wave vectors up to $2G_{cut}$ where $E_{cut} = \frac{\hbar^2}{2m_e}G_{cut}^2$. The Kohn-Sham ground states were calculated via either a Davidson block iteration scheme[50] or a combination of the Davidson scheme with a residual minimization method, direct inversion in the iterative subspace (RMM-DIIS) scheme.[51,52] The break point for the electronic self-consistency loop in the higher-accuracy single-point calculations was an energy difference of less than 1.0×10^{-7} eV.

For the slab calculations, the dipole was calculated in the surface normal direction and a compensating linear electrostatic potential was added to the local potential in the void region of the supercell in order to correct for the errors introduced by the use of periodic boundary conditions with asymmetric slab models.[53] A Bader charge analysis was carried out on the overlayers to estimate the charge transfer to or from the adsorbed mercury atoms.[54]

In order to calculate the work function, the plane-average electrostatic potential along the surface normal was computed; the work function Φ was computed for clean and mercury-covered surfaces as $\Phi = V_0 - E_F$ where E_F is the Fermi energy and V_0 is the value of the electrostatic potential in the void region of the supercell, which mimics the vacuum.[55,56] The computed values of Φ for the clean, relaxed surfaces are included in the supplementary information.[48]

The k points were chosen according to the Monkhorst Pack scheme.[57] Convergence with k-point sampling was investigated for the (1×1)-Hg/Pd(100) overlayer; results are presented in the supplementary information.[48] The energy of adsorption is converged to within ± 0.02 eV even with the $6 \times 6 \times 1$ grid. For subsequent calculations on the (1×1)-Hg/M(100) supercell, an $8 \times 8 \times 1$ Monkhorst-Pack grid was employed. A $6 \times 6 \times 1$ Monkhorst-Pack grid has been used for integration in reciprocal space for all other supercells except for the relatively large $(2\sqrt{3} \times 3)$-Hg/M(111) overlayer, for which a $4 \times 6 \times 1$ grid was chosen. Based on the data presented in the supplementary information,[48] the calculated work function for the production calculations may be considered converged only to within approximately ± 0.05 eV for the bare metal surfaces and ± 0.15 eV for the mercury overlayers.

Convergence as a function of the size of the plane-wave basis set was investigated using the (1×1)-Hg/Pd(001) model. The results, presented in the supplementary information,[48] confirm that both the energy of adsorption and the work function are converged to within ± 0.01 eV with respect to the basis set for $E_{cut} = 330$ eV. For all subsequent calculations, a basis set consisting of plane waves with energy up to $E_{cut} = 380$ eV was used.

TABLE I. Binding enegies (in eV) for high-symmetry sites on the $c(4 \times 4)$−Hg/Au(001) 0.125 ML overlayer calculated using the PBE, PW91, and LDA functionals. Results of cluster relativistic DFT calculations of Sarpe-Tudoran *et al.* (Ref. 27) are presented for comparison.

Site	E_{ads} (PBE)	E_{ads} (PW91)	E_{ads} (LDA)	E_{ads} (Ref. 27)
Hollow	−0.61	−0.66	−1.48	−0.84
Bridge	−0.47	−0.50	−1.11	−1.52
Top	−0.36	−0.39	−0.84	−1.02

Calculations on the bare and Hg-covered (1×1)-Hg/Pd(001) overlayers were carried out with various numbers of layers in the metal slab in order to examine convergence with respect to the number of layers in the slab. Results are presented in the supplementary information.[48] The binding energy, work function for the bare metal, and change in work function upon Hg adsorption are converged to within a factor of ± 0.03, ± 0.05, and ± 0.08 eV, respectively, with a four-layer slab. Since the cost of the calculations scales steeply with system size, four-layer slabs were used for subsequent calculations.

IV. RESULTS: MERCURY ON METAL SURFACES

Hollow, top, and bridge sites were investigated for all the overlayers included in this study. Representative results are presented (in Table I) for low coverage on the the Au(001) surface using three functionals (LDA, PW91, and PBE). The PW91 and PBE functionals yield very similar results while the LDA, as is common, shows significant overbinding. Binding at the hollow sites was preferred, followed by the bridge site, with the top site being the least favored, for all overlayers included in this study. The differences in adsorption energies for mercury at the fcc and hcp hollow sites on the (111) surfaces were negligible. All data presented hereafter are for adsorption at hollow sites and were generated using the PBE functional.

Mercury is predicted to bind to Ag, Au, Cu, Ni, Pd, and Pt with binding energies between −0.30 and −1.10 eV. Binding energies of this order of magnitude are sizable and denote chemical interactions between the metal surfaces and adsorbed mercury. Of the six metals studied here, DFT predicts that Pd and Pt bind Hg atoms the most strongly (E_{ads}= −0.58 to −1.10 eV), followed by Ni and Cu (E_{ads}= −0.48 to −0.82 eV). Ag and Au bind Hg the most weakly (E_{ads}=−0.30 to −0.51 eV).

For all metal surfaces studied in this work except Ag(001), the adsorption of mercury is predicted to cause a negative change in the work function. The change in work function is calculated to be positive or minimally negative for Ag(001) surfaces, significantly negative ($\Delta\Phi \approx$ −0.25 to −0.85 eV) for Ag(111), Au, Cu, and Ni, and sizably negative ($\Delta\Phi \approx$−0.1 to −1.5 eV) for higher coverages on Pd and, especially, Pt. The binding energies for mercury on palladium and to platinum are very similar, but the change in work function is calculated to be almost twice as large on

TABLE II. Hg adsorption on (111) metal surfaces on hollow sites: θ denotes coverage, E_{ads} denotes binding energy, M-Hg and Hg-Hg denote distances between adsorbed Hg and substrate or neighboring Hg atoms, respectively, Φ is the calculated work function of the bare metal, and $\Delta\Phi$ and ΔQ are the adsorption-induced changes in work function and charge on Hg.

Overlayer	θ (ML)	E_{ads} (eV)	M-Hg (Å)	Hg-Hg (Å)	Φ (eV)	$\Delta\Phi$ (eV)	ΔQ (a.u.)
$(2\sqrt{3}\times 3)$-Hg/Ag(111)	0.083	−0.34	3.00	8.83	4.48	−0.24	−0.03
$(2\sqrt{3}\times 3)$-Hg/Au(111)	0.083	−0.36	2.99	8.85	5.16	−0.37	−0.13
$(2\sqrt{3}\times 3)$-Hg/Cu(111)	0.083	−0.52	2.75	7.70	4.79	−0.44	−0.02
$(2\sqrt{3}\times 3)$-Hg/Ni(111)	0.083	−0.67	2.72	7.47	5.08	−0.51	0.06
$(2\sqrt{3}\times 3)$-Hg/Pd(111)	0.083	−0.84	2.81	8.41	5.27	−0.42	−0.15
$(2\sqrt{3}\times 3)$-Hg/Pt(111)	0.083	−0.75	2.86	8.44	5.70	−0.61	−0.22
$p(2\times 2)$-Hg/Ag(111)	0.25	−0.36	3.01	5.88	4.47	−0.38	−0.02
$p(2\times 2)$-Hg/Au(111)	0.25	−0.38	3.01	5.90	5.27	−0.76	−0.12
$p(2\times 2)$-Hg/Cu(111)	0.25	−0.53	2.78	5.14	4.84	−0.59	0.00
$p(2\times 2)$-Hg/Ni(111)	0.25	−0.64	2.74	4.98	5.09	−0.82	−0.03
$p(2\times 2)$-Hg/Pd(111)	0.25	−0.81	2.83	5.61	5.31	−0.84	−0.12
$p(2\times 2)$-Hg/Pt(111)	0.25	−0.68	2.88	5.62	5.67	−1.06	−0.18
$(\sqrt{3}\times\sqrt{3})R30°$-Hg/Ag(111)	0.333	−0.31	3.06	5.08	4.43	−0.35	−0.01
$(\sqrt{3}\times\sqrt{3})R30°$-Hg/Au(111)	0.333	−0.32	3.05	5.09	5.14	−0.59	−0.09
$(\sqrt{3}\times\sqrt{3})R30°$-Hg/Ci(111)	0.333	−0.48	2.82	4.43	4.74	−0.56	−0.02
$(\sqrt{3}\times\sqrt{3})R30°$-Hg/Ni(111)	0.333	−0.61	2.76	4.30	5.06	−0.80	0.01
$(\sqrt{3}\times\sqrt{3})R30°$-Hg/Pd(111)	0.333	−0.80	2.83	4.84	5.28	−0.88	−0.11
$(\sqrt{3}\times\sqrt{3})R30°$-Hg/Pt(111)	0.333	−0.67	2.89	4.85	5.70	−1.16	−0.15
$p(2\times 2)$-Hg/Ag(111)	0.5	−0.37	3.09	3.40	4.47	−0.25	0.01
$p(2\times 2)$-Hg/Au(111)	0.5	−0.35	3.11	3.41	5.29	−0.66	−0.08
$p(2\times 2)$-Hg/Cu(111)	0.5	−0.51	2.87	2.97	4.85	−0.32	0.02
$p(2\times 2)$-Hg/Ni(111)	0.5	−0.61	2.75	2.88	5.08	−0.50	0.00
$p(2\times 2)$-Hg/Pd(111)	0.5	−0.81	2.85	3.24	5.31	−0.91	−0.07
$p(2\times 2)$-Hg/Pt(111)	0.5	−0.69	2.92	3.25	5.68	−1.05	−0.12

platinum as on palladium. Silver and gold compare to one another in an analogous way; their binding energies are similar to one another (although much smaller than those of platinum and palladium) but the work function change on gold is about double the size of the work function change on silver.

A. Hg on (111) metal surfaces

Adsorption of Hg on (111) metal surfaces was calculated for four overlayers ranging from 0.0833 ML to 0.5 ML. The results for mercury adsorption on (111) metal surfaces are presented in Table II and the overlayers are represented in Fig. 1. For each overlayer, the mercury-mercury distances (Hg-Hg) result from the imposition of periodic boundary conditions and therefore are a direct function of the size of the lattice constant for any given overlayer pattern. The $(2\sqrt{3}\times 3)$-Hg/M(111) 0.0833 ML overlayer is the largest supercell considered in this study. Distances between neighboring adsorbed mercury atoms on this overlayer are between 7.47 Å (on the nickel surface) and 8.85 Å (on the gold surface); these separations are large enough such that the results should be dominated by Hg-metal effects, rather than Hg-Hg effects. As can be observed in Fig. 1, the $p(2$

$\times 2)$-Hg/M(111) 0.25 ML, $(\sqrt{3}\times\sqrt{3})R30°$-Hg/M(111) 0.333 ML, and $p(2\times 2)$-Hg/M(111) 0.5 ML all have Hg atoms situated in a symmetric hexagonal pattern [although in the $p(2\times 2)$-Hg/M(111) 0.5 ML overlayer, there is not an Hg atom in the center of each hexagon, while for the former overlayers, there is]. The supercell used for the $p(2 \times 2)$-Hg/M(111) 0.25 ML overlayer and the $p(2 \times 2)$-Hg/M(111) 0.5 ML overlayer is the same, with one and two Hg atoms included, respectively, for the overlayers. The calculations predict binding of Hg to all six metals in all four overlayers to be thermodynamically favored. Adsorption of mercury is predicted to cause a decrease in the work function on all six metals and for all the overlayers, with the most dramatic changes occurring on platinum.

B. Hg on (001) metal surfaces

Adsorption of mercury on the (001) metal surfaces was investigated for three overlayers with coverages ranging from 0.125 to 1.0 ML. The results for the (001) surfaces are presented in Table III and the overlayers are represented in Fig. 2. In contrast to the overlayers on the (111) surfaces, the
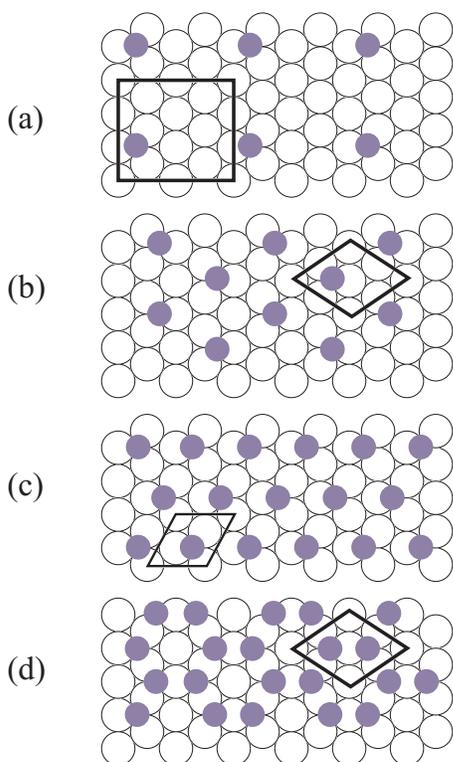
FIG. 1. (Color online) Hg overlayers on fcc (111) metal surfaces: (a) $(2\sqrt{3}\times3)$-Hg/M(111) overlayer, 0.083 ML; (b) $p(2\times2)$-Hg/M(111) overlayer, 0.25 ML; (c) $(\sqrt{3}\times\sqrt{3})R30°$-Hg/$M$(111) overlayer, 0.333 ML; (d) $p(2\times2)$-Hg/M(111) overlayer, 0.50 ML. Open circles represent substrate atoms and solid circles represent adsorbed mercury atoms (in threefold hollow positions). Refer to Table II.

Hg atoms on the (001) surface are arranged in rectilinear patterns. The $c(4\times4)$-Hg/M(001) overlayer (0.125 ML) is the lowest coverage modeled on the (001) surface. Hg-Hg distances are 7.04–8.35 Å on the surface; these distances are large enough that results for this overlayer should be dominated by Hg-metal interactions.

For any given metal, the binding of mercury is stronger on the (001) surface as compared to the (111) surface (with two exceptions noted below). On the (111) surface, mercury is bound in the threefold hollow sites, while on the (001) surface, it is bound in the fourfold hollow sites, giving the adsorbed mercury a (favorable) higher coordination number on the (001) surfaces. Absorption of Hg on all six metals is thermodynamically favored except for the $c(1\times1)$-Hg/Cu(001) and $c(1\times1)$-Hg/Ni(001) overlayers. These model a full monolayer on metals in which the relatively small lattice constants bring the adsorbed Hg atoms too close together on the surface, leading to repulsive Hg-Hg interactions.

The calculated change in work function upon adsorption of mercury is negative for all overlayers on all six metal (001) substrates except for the $c(2\times2)$ and $c(1\times1)$ overlayers on Ag.

V. DISCUSSION

A. Magnitude of the interaction with metal surfaces

The magnitude of the interaction between mercury and the metal surface is more strongly influenced by the identity of the substrate than any other factor considered here (such as the distance between neighboring Hg atoms or the amount of charge that is transferred from the mercury atom to the metal surface). All the mercury overlayers examined here are thermodynamically favored with the exception only of two overlayers in which mercury atoms are forced to reside within a distance of 2.6 Å of one another.

The results of this study indicate a general ordering of the metal surfaces with increasing reactivity towards mercury according to Ag<Au<Cu<Ni<Pt<Pd. This is in agreement with the results of Soverna and colleagues, with the exception of Ni, which they found interacted with mercury more weakly than Au. Soverna and colleagues pointed out that oxygen may have been present on the surface of the metal under the conditions of their experiment and this could have caused the difference.

Quantitative agreement between the DFT results and experimental data is good for the $c(4\times4)$-Hg/Cu(001) and $c(2\times2)$-Hg/Cu(001) overlayers, for which the theoretical (experimental) E_{ads} are −0.67 (−0.70) and −0.71 (−0.74) eV, respectively.[32] Agreement for the $c(1\times1)$-Hg/Ag(001) surface is fair, with theoretical (experimental) E_{ads} of −0.30 (−0.63) eV.[32] The agreement for the nickel (001) and (111) surface overlayers is poor overall. The theoretical (experimental) E_{ads} for the ($\sqrt{3}$
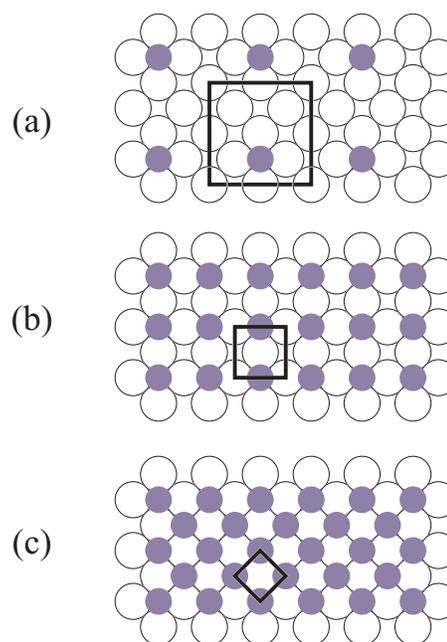
FIG. 2. (Color online) Models for Hg adsorption on fcc (001) metal surfaces: (a) $c(4\times4)$-Hg/M(001) overlayer, 0.125 ML; (b) $c(2\times2)$-Hg/M(001) overlayer, 0.5 ML; (c) $c(1\times1)$-Hg/M(001) overlayer, 1.0 ML. Open circles represent substrate atoms and solid circles represent adsorbed mercury atoms (in fourfold hollow positions). Refer to Table III.

TABLE III. Hg adsorption on (001) metal surfaces on hollow sites: θ denotes coverage, E_{ads} denotes binding energy, M-Hg and Hg-Hg denote distances between adsorbed Hg and substrate or neighboring Hg atoms, respectively, Φ is the calculated work function of the bare metal, and $\Delta\Phi$ and ΔQ are the adsorption-induced changes in work function and charge on Hg.

Overlayer	θ (ML)	E_{ads} (eV)	M-Hg (Å)	Hg-Hg (Å)	Φ (eV)	$\Delta\Phi$ (eV)	ΔQ (a.u.)
$c(4\times4)$-Hg/Ag(001)	0.125	−0.50	3.01	8.32	4.21	−0.09	0.01
$c(4\times4)$-Hg/Au(001)	0.125	−0.61	2.94	8.35	5.04	−0.28	−0.09
$c(4\times4)$-Hg/Cu(001)	0.125	−0.67	2.78	7.26	4.55	−0.32	0.03
$c(4\times4)$-Hg/Ni(001)	0.125	−0.82	2.73	7.04	4.89	−0.45	0.02
$c(4\times4)$-Hg/Pd(001)	0.125	−1.10	2.83	7.93	5.09	−0.35	−0.05
$c(4\times4)$-Hg/Pt(001)	0.125	−1.09	2.83	7.95	5.65	−0.67	−0.18
$c(2\times2)$-Hg/Ag(001)	0.5	−0.51	3.02	4.16	4.17	0.03	0.06
$c(2\times2)$-Hg/Au(001)	0.5	−0.51	3.00	4.17	5.22	−0.90	−0.10
$c(2\times2)$-Hg/Cu(001)	0.5	−0.71	2.80	3.63	4.71	−0.58	0.04
$c(2\times2)$-Hg/Ni(001)	0.5	−0.81	2.77	3.52	4.93	−0.60	0.04
$c(2\times2)$-Hg/Pd(001)	0.5	−1.08	2.83	3.97	5.07	−0.80	−0.03
$c(2\times2)$-Hg/Pt(001)	0.5	−0.97	2.85	3.98	5.59	−1.42	−0.04
$c(1\times1)$-Hg/Ag(001)	1.0	−0.30	3.30	2.94	4.08	0.04	0.01
$c(1\times1)$-Hg/Au(001)	1.0	−0.35	3.39	2.95	5.11	−0.76	−0.07
$c(1\times1)$-Hg/Cu(001)	1.0	0.27	3.14	2.57	4.66	−0.59	0.01
$c(1\times1)$-Hg/Ni(001)	1.0	0.55	2.99	2.49	4.90	−0.61	0.00
$c(1\times1)$-Hg/Pd(001)	1.0	−0.67	2.95	2.80	5.05	−0.66	−0.06
$c(1\times1)$-Hg/Pt(001)	1.0	−0.58	3.05	2.81	5.58	−0.90	−0.10

$\times\sqrt{3})R30°$-Hg/Ni(111) and $p(2\times2)$-Hg/Ni(001) overlayers are −0.61 (−2.07) and −0.61 (−0.83) eV, respectively.[31] The theoretical (experimental) E_{ads} for the $c(2\times2)$-Hg/Ni(001) overlayer is −0.81 (−1.71) eV.[28] Overall, the DFT results using the PBE functional give values for E_{ads} that are low in comparison with experiment. If one compares the thermochromatic studies of mercury adsorption of Soverna *et al.* with the most strongly bound overlayer considered in this study [$c(4\times4)$-Hg/M(001)], it appears the PBE functional is underestimating the strength of the interaction by 0.1–0.4 eV.[35] Use of the LDA functional would provide stronger interactions; however, judging by the results presented in Table I, the interaction would almost certainly be overestimated by about the same amount.

B. Site preference

Using standing x-ray wave-field absorption experiments, Prince *et al.* deduced that Hg atoms are bound at the bridge site on the $c(2\times2)$-Hg/Ni(001) surface.[30] However, these authors assumed an Hg-Ni distance of 2.63 Å. They point out that adsorption at the hollow sites would be consistent with their data if the Hg-Ni bond were $\approx 2.95\pm0.10$ Å; the Hg-Ni distance for this overlayer that is determined by the DFT calculations is 2.77 Å. Subsequently, Poulsen *et al.* used transmission channeling to determine that adsorption of Hg on Ni(001) below 0.5 ML occurs at the four-fold hollow sites at a height of 2.25 ± 0.10 Å.[34] The DFT results presented here are consistent with this result. As can be seen in

Table I, the energy ordering of the high-symmetry surface sites remains consistent whether the LDA, PW91, or PBE functional is used.

The magnitude of the interactions and the energy ordering of the high-symmetry sites on metal surfaces presented in this work differ from those reported for Hg on Au(001) by Sarpe-Tudoran and colleagues, whose relativistic DFT calculations were performed on cluster models and embedded clusters.[27] Sarpe-Tudoran *et al.* report the bridge site as the lowest-energy binding site for mercury on Au(001), while in the present study, the hollow site was found to be more thermodynamically favorable for Hg on all six metal surfaces. Sarpe-Tudoran *et al.* point out that, due to the extreme demands of the relativistic calculations, they were not able to ensure that the results were converged with respect to cluster size. In the present work, the slab models do not suffer from size limitations, but relativistic effects are accounted for only in the use of the PAW pseudopotentials, which are based on scalar-relativistic all-electron calculations. Differences in the energy ordering of high-symmetry surface sites may also be due to limitations of the DFT formalism. There have been cases in which the site preference for adsorption on metals has been incorrectly predicted by DFT, possibly as a result of the incorrect energies of unoccupied bands associated with adsorbates in cases where back-donation from the metal to the adsorbate is important.[58,59]

C. Lateral Hg-Hg interactions

As coverage is increased and Hg adatoms are brought closer to one another on the metal surfaces, there is evidence
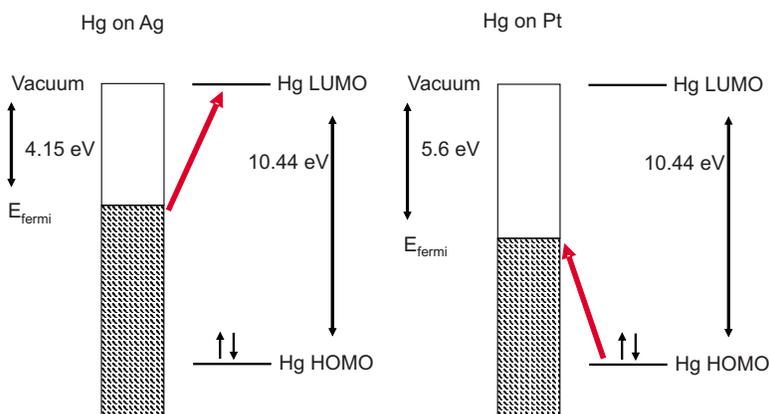
FIG. 3. (Color online) Koopmans' theorem interpretation for the relationship between the magnitude of the work function change and the value of the work function for the bare metal.

for first attractive and then repulsive interactions. Attractive Hg-Hg interactions were proposed in order to explain experimental observations in several previous works.[28,31,32] The current DFT results are consistent with the existence of weak attractive Hg-Hg interactions. For example, in going from the $c(4 \times 4)$ to the $c(2 \times 2)$ phase on the Cu(001) surface, there is a small energetic advantage of −0.04 eV. This corresponds to bringing surface Hg atoms from a separation of 7.26 to 3.63 Å. This is very close to the Hg-Hg separation in the gas-phase Hg_2 dimer.[60] The binding energy of the Hg_2 dimer, as calculated using plane-wave DFT, is ∼−0.033 eV at an Hg-Hg separation of 3.60 Å.

Strong short-range repulsive lateral Hg-Hg interactions are consistent with the decrease in binding energy with increased coverage and with the result that the $c(1 \times 1)$ over-

layer is not thermodynamically favored on either Cu(001) or Ni(001) because these overlayers would require Hg-Hg distances of less than 2.6 Å.

D. Change in work function

The adsorbate-induced change in work function is negative for every overlayer studied here with the exception of the $c(2 \times 2)$-Hg/Ag(001) and $c(1 \times 1)$-Hg/Ag(001) overlayers. The adsorbate-induced change in the work function is influenced by the change in the effective surface dipole.[55] The surface dipole is affected by factors such as charge spill-out and Smoluchowski smoothing, which tend to balance one another. For an electropositive adsorbate such as mercury,
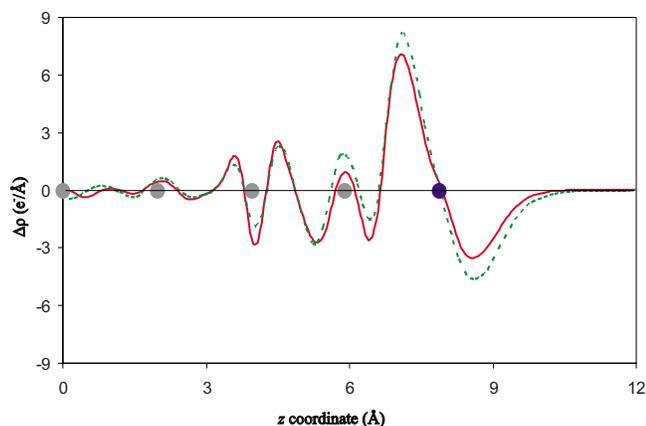
FIG. 4. (Color online) Adsorbate-induced charge density difference as a function of z coordinate for the $c(4 \times 4)$-Hg/M(001) overlayer, M=Pd, solid line (red); Pt, dashed line (green). Positive values indicate charge is accumulated upon adsorption while negative values indicate loss of charge upon Hg adsorption. The location of the adsorbed Hg atom is indicated by a dark (blue) dot; the locations of the layers of the substrate metal atoms are indicated by light (gray) dots. The vacuum region of the supercell has been omitted for clarity.
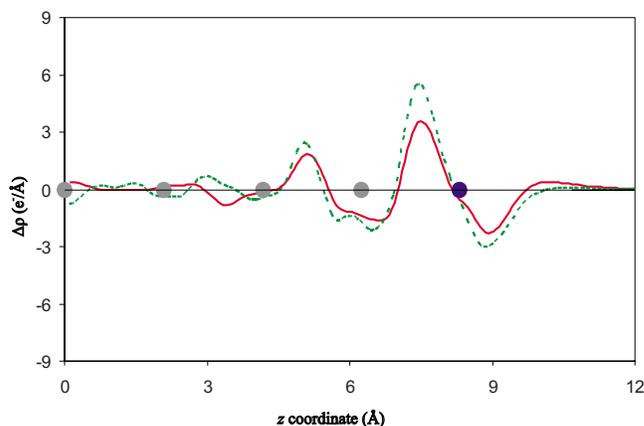
FIG. 5. (Color online) Adsorbate-induced charge density difference as a function of z coordinate for the $c(4 \times 4)$-Hg/M(001) overlayer, M=Ag, solid line (red); Au, dashed line (green). Positive values indicate charge is accumulated upon adsorption while negative values indicate loss of charge upon Hg adsorption. The location of the adsorbed Hg atom is indicated by a dark (blue) dot; the locations of the layers of the substrate metal atoms are indicated by light (gray) dots. The vacuum region of the supercell has been omitted for clarity.

surface Ag atoms

Hg
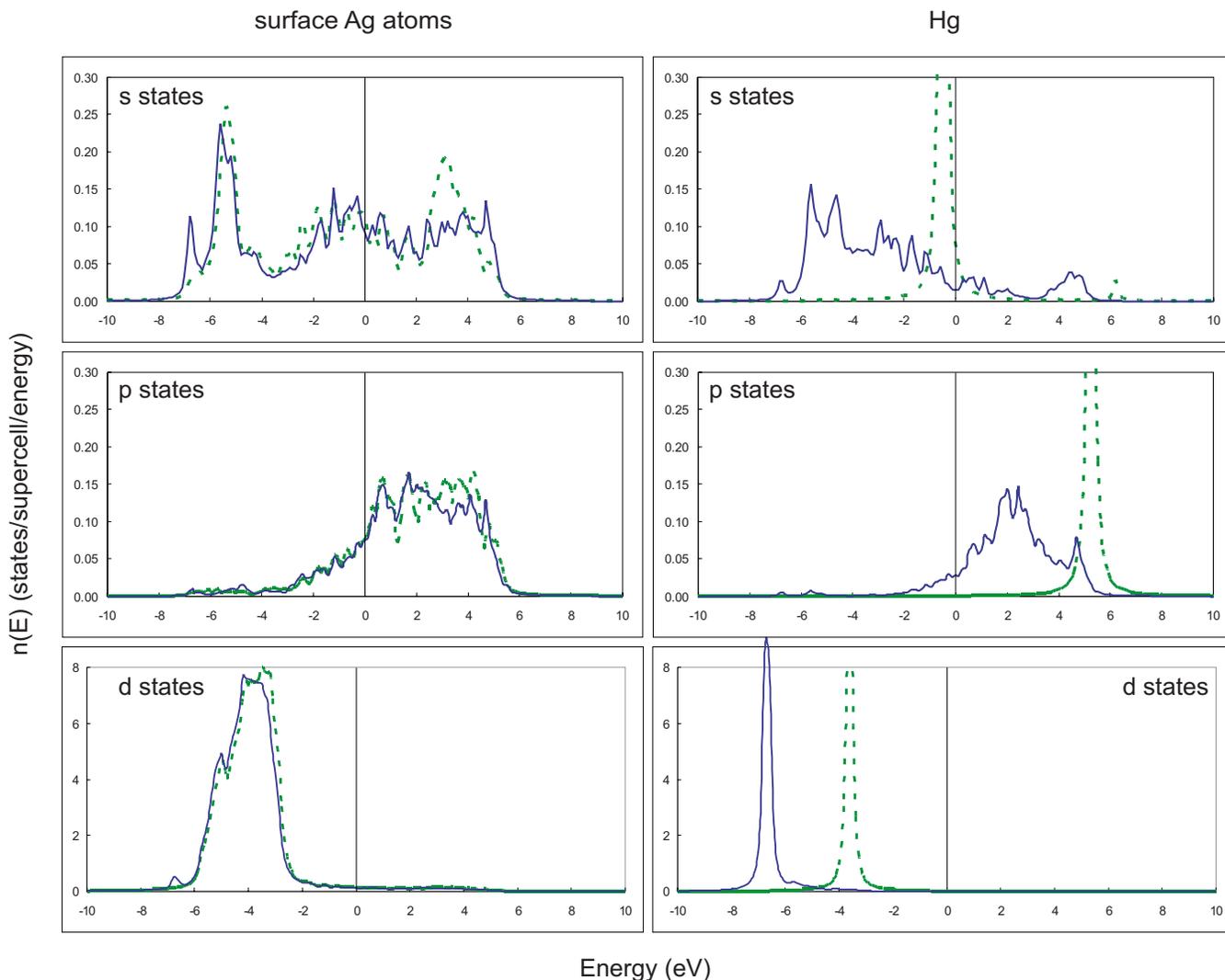
FIG. 6. (Color online) Site-projected density of states (states/atom/energy) for Hg on the $c(4\times4)$-Hg/Ag(001) overlayer. The s, p, and d states of the four metal surface atoms before adsorption (dotted green line) and after adsorption (solid blue line) are presented on the left. On the right are presented the s, p, and d states for an isolated Hg atom (dotted green line) and Hg adsorbed in the fourfold hollow sites of the metal surface (solid blue line).

there is typically charge transfer from the adsorbate into the substrate, resulting in a decrease in the work function. It can be determined by examination of the data in Tables II and III that the adsorbate-induced change in work function is dramatic for mercury adsorption on the metals with larger work functions—e.g., Pd and Pt. A simple interpretation for this relation is possible via Koopmans' theorem.[61,62] The electron affinity of mercury is nearly zero, so we can set the level of the Hg lowest unoccupied molecular orbital (LUMO) to the level of the vacuum for the metal surface. The Hg highest occupied molecular orbital (HOMO) then should be below the LUMO by approximately the amount of the ionization potential for mercury, which is 10.44 eV. In the case of metals having fairly large work functions such as Pd and Pt, the energy difference between the HOMO and the Fermi level should be smaller than between the Fermi level and the LUMO, leading to charge transfer from the HOMO to the metal substrate. For metals with smaller work functions such as Ag, the energy difference between the Fermi level and the LUMO might be small enough to lead to charge transfer from the metal substrate into the LUMO of mercury. This is illustrated in Fig. 3. The values of ΔQ calculated via the Bader analysis are also consistent with this view, being typically most negative for the Pd and Pt overlayers.

E. Charge density differences

To investigate the changes in the charge density that result from the adsorption of mercury to the metal surfaces, the charge density difference along z has been calculated. The plane-averaged charge density $\rho(z)$ is given by

$$\rho(z) = \frac{1}{A}\int_0^{a_1} dx \int_0^{a_2} dy \rho(x,y,z), \qquad (1)$$

where A is the surface area of the supercell, a_1 and a_2 are the supercell dimensions in x and y, and $\rho(x,y,z)$ is the full
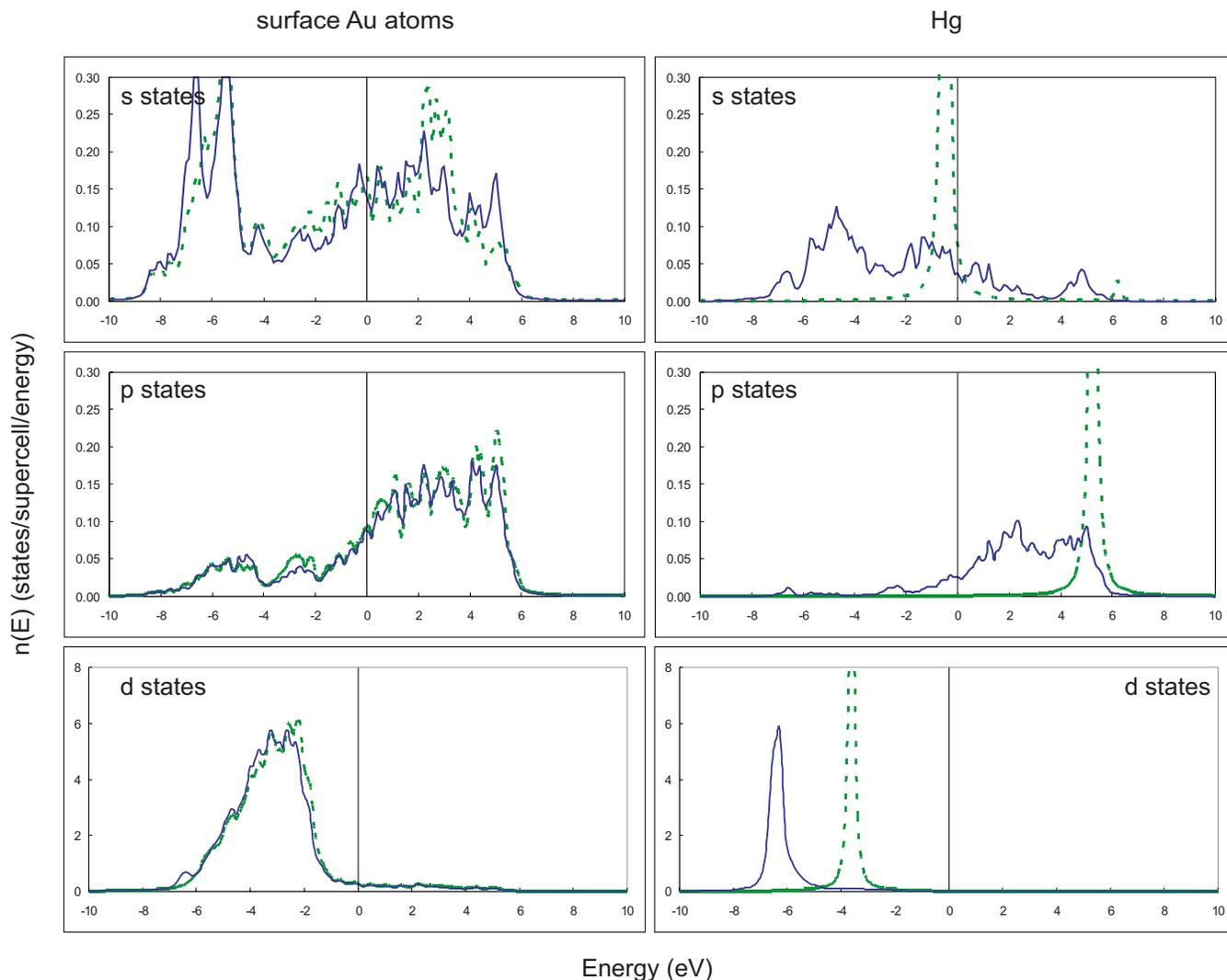
FIG. 7. (Color online) Site-projected density of states (states/atom/energy) for Hg on the $c(4\times4)$-Hg/Au(001) overlayer. The s, p, and d states of the four metal surface atoms before adsorption (dotted green line) and after adsorption (solid blue line) are presented on the left. On the right are presented the s, p, and d states for an isolated Hg atom (dotted green line) and Hg adsorbed in the fourfold hollow sites of the metal surface (solid blue line).

charge density. The change in charge density upon adsorption of mercury has been calculated as

$$\Delta\rho(z) = \rho(z) - [\rho_{surf}(z) + \rho_{Hg}(z)], \qquad (2)$$

where $\rho(z)$ is the charge density along z for the metal surface with Hg adsorbed, $\rho_{surf}(z)$ is the charge density along z of the surface metal atoms, in the same positions but with the mercury atom removed, and $\rho_{Hg}(z)$ is the charge density along z of the Hg atom with the surface metal atoms removed.[55]

It is interesting to examine the similarities and differences for mercury adsorption to Pd and Pt. Binding energies for mercury are similar for these two substrates, but the change in the work function and the value of ΔQ is dramatically larger for Pt in all the overlayers considered. The lattice constants are quite similar with $a=3.965$ Å for Pd and $a=3.977$ Å for Pt. For the $c(4\times4)$-Hg/M(001) overlayer, $E_{ads}=-1.10$ (−1.09) eV for Pd (Pt). $\Delta\Phi=-0.35$ eV for Pd,

but for Pt it is −0.67 eV, almost twice as large. The Bader charge analysis of the charge density shows that $\Delta Q=-0.05e$ for Pd while, for Pt, $\Delta Q=-0.18e$. In both cases, there is adsorbate-induced charge transfer from mercury to the metal, but for Pt it is several times larger.

The charge density difference upon adsorption of Hg on Pd and Pt is presented in Fig. 4. Positive values signify accumulation of charge upon adsorption; negative values indicate locations where charge density is lost upon Hg adsorption. The vacuum region of the supercell has been omitted for clarity. Changes in the charge density are most pronounced in the immediate region of the adsorbed Hg atom and the first two metal substrate layers. Adsorption of Hg induces a large transfer of charge from the region above the Hg to the region between the Hg atom and the first layer of the substrate metal. Around the first layer of the metal substrate there is an adsorbate-induced increase of charge density, while around the second layer there is an adsorbate-

surface Pd atoms

Hg
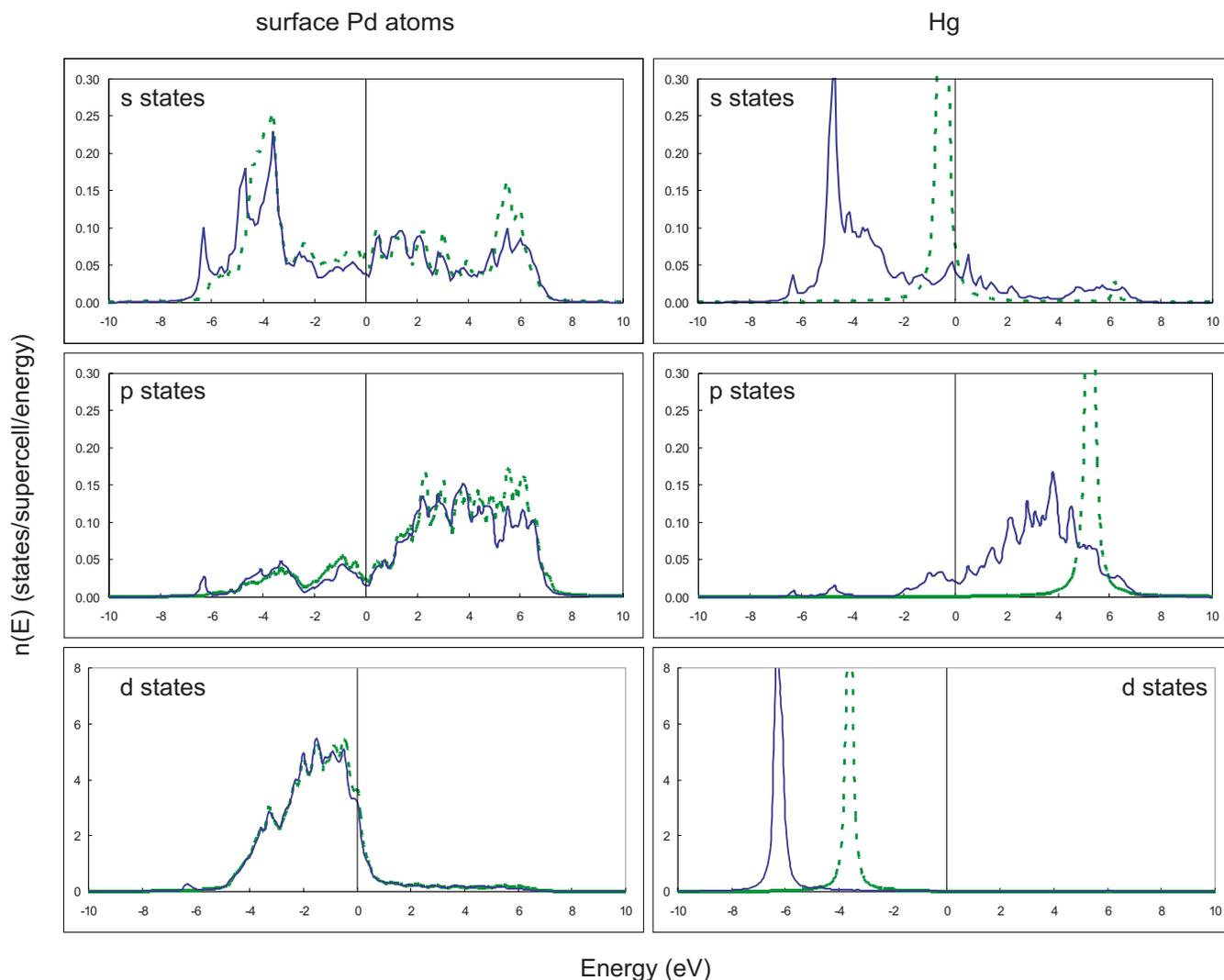
FIG. 8. (Color online) Site-projected density of states (states/atom/energy) for Hg on the $c(4 \times 4)$-Hg/Pd(001) overlayer. The s, p, and d states of the four metal surface atoms before adsorption (dotted green line) and after adsorption (solid blue line) are presented on the left. On the right are presented the s, p, and d states for an isolated Hg atom (dotted green line) and Hg adsorbed in the fourfold hollow sites of the metal surface (solid blue line).

induced reduction of charge density. The oscillatory pattern of the charge density difference is much diminished by the third layer of the metal substrate. The overall pattern of the charge density difference for Pd and Pt is qualitatively similar, but the amount of charge transferred to the substrate from the Hg atom is greater in the case of Pt. This is consistent with the much greater $\Delta\Phi$ and ΔQ for Pt as compared with Pd, despite the similarity in the value of E_{ads} for these two metal substrates.

Charge density differences for the $c(4 \times 4)$-Hg/M(001), M=Ag, Au, overlayers are presented in Fig. 5. $E_{ads}=$ −0.50 eV for Ag while, for Au, E_{ads}=−0.61 eV. Thus mercury binds more weakly to both Ag and Au in contrast with Pd and Pt. The change in the work function and the values of ΔQ for Ag (Au) are −0.09 (−0.28) eV and +0.01e (−0.09e), respectively. Examination of the charge density differences reveals that charge is transferred from the region above the mercury to the region between the mercury and the first sub-

strate layer, but overall the charge transfer is not as dramatic as what was observed for Pd and Pt. Another difference is that charge is lost from the area around the first metal substrate Ag and Au atoms, in contrast to Pd and Pt, where charge was gained around the first layer substrate metal atoms. The accumulation of charge is mostly in the region between the adsorbate and the surface. It is also interesting to note that there is a small accumulation of charge in the region approximately 2–3 Å above the mercury atom, which would be consistent with charge transfer into the LUMO of the mercury atom as suggested by the Koopmans' theorem interpretation. This is more pronounced for Ag than for Au, which is consistent with the fact that the work function for Ag is smaller than that of Au.

F. Partial density of states

In order to examine the partial density of states (PDOS), the wave functions have been projected onto spherical har-
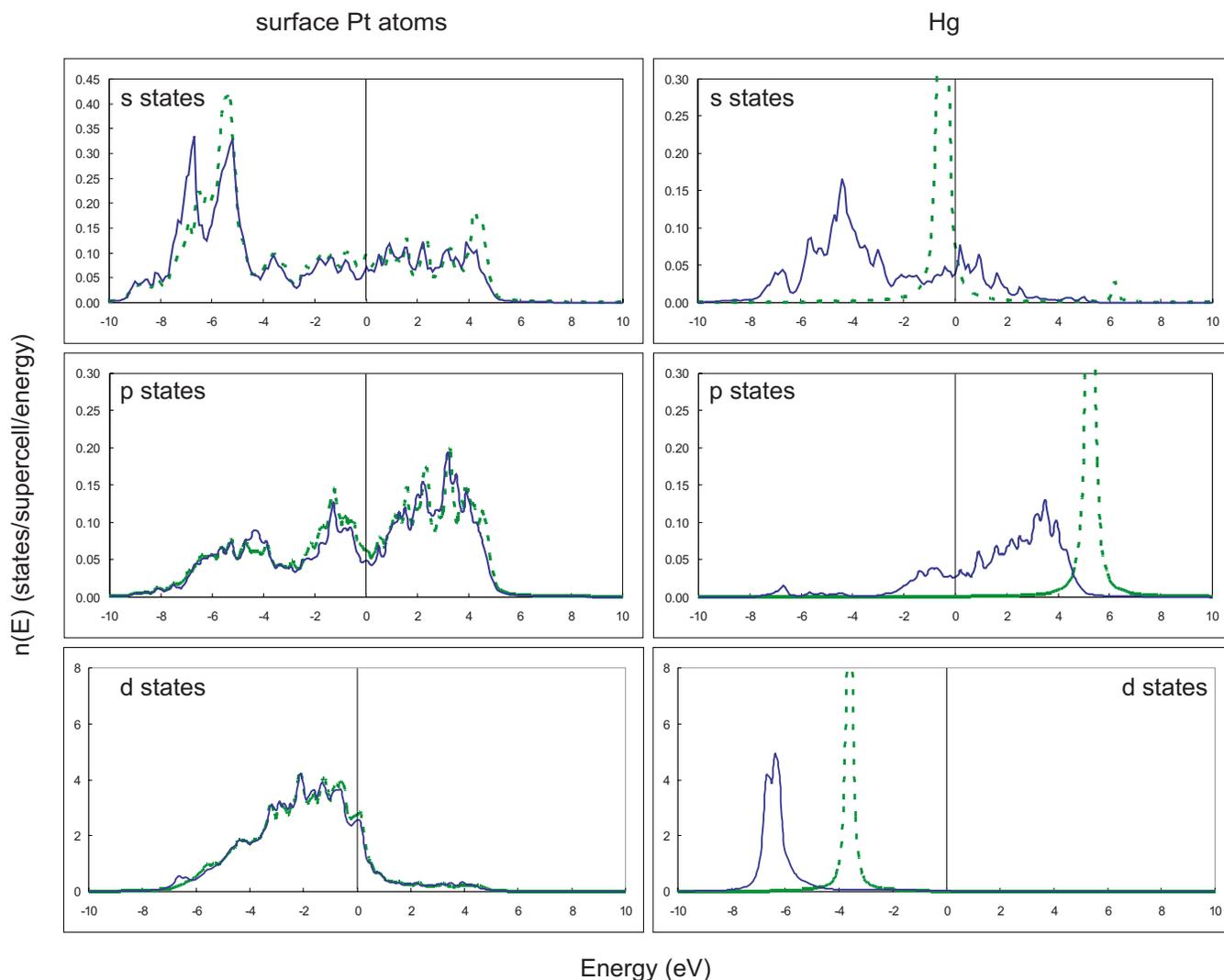
FIG. 9. (Color online) Site-projected density of states (states/atom/energy) for Hg on the $c(4 \times 4)$-Hg/Pt(001) overlayer. The s, p, and d states of the four metal surface atoms before adsorption (dotted green line) and after adsorption (solid blue line) are presented on the left. On the right are presented the s, p, and d states for an isolated Hg atom (dotted green line) and Hg adsorbed in the fourfold hollow sites of the metal surface (solid blue line).

monics centered on the Hg atom and the four metal substrate atoms that form the fourfold hollow site for the Hg adsorption for the $c(4 \times 4)$-Hg/M(001) overlayer, M=Ag, Au, Pd, and Pt overlayers. The partial density of states are presented in Figs. 6–9.

The DOS of the isolated Hg atom [calculated in a $(20 \text{ Å})^3$ supercell with periodic boundary conditions] is characterized by well-defined d and s states near -3.6 and -0.5 eV, respectively, and an (unfilled) p state near 5.3 eV. After adsorption on the metal surfaces, the s and p states are markedly broadened and lowered, indicating strong interactions with the metal. The p states after adsorption exhibit a shoulder extending below the Fermi level; i.e., there are filled p states in the adsorbed Hg atom. As mentioned above, the charge density difference showed evidence for charge transfer into the LUMO of Hg on the Au and Ag surfaces. Integration of the filled p states in the adsorbed Hg atom indicates that the amount of charge transferred to the Hg atom via this trans-

formation is small and similar across the four metals examined here. However, the Wigner-Seitz radius for Hg used for the decomposition of the density of states (1.614 Å) is unfortunately too small to extend into the area where charge donation from the metal to Ag and Au was observed in the charge density difference shown in Fig. 5.

The d bands for bare Ag and Au do not have states at the Fermi level, while Pd and Pt have a large Fermi-level surface density of states. The d-band centers for the bare Ag, Au, Pd, and Pt surface atoms are located at -3.96, -3.27, -1.82, and -2.43 eV, respectively, before adsorption of Hg. There is a rough correlation between the level of the d band center for the bare metal surface atoms and the binding energy of Hg to the surface (presented in Fig. 10) with the metals for which the d band is lower exhibiting weaker binding for Hg. The d bands are slightly lowered in all four cases, to -4.10, -3.42, -1.89, and -2.50 eV, respectively. The d-band shift is more pronounced for Ag and Au. Hg adsorption induces a reso-
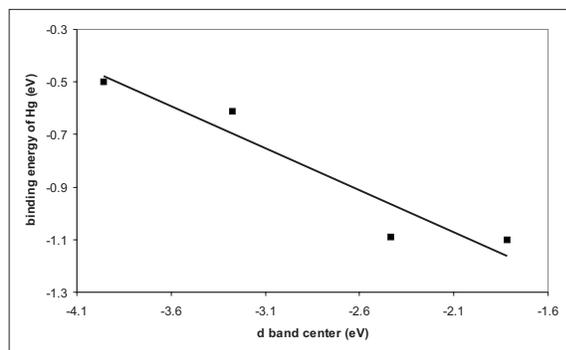
FIG. 10. E_{ads} for the $c(4 \times 4)$-Hg/M(001) overlayer, M=Ag, Au, Pd, and Pt plotted versus the d-band center for the bare surface metal atoms.

nance observable near -6.5 eV, the energy of the d band for adsorbed Hg, in the s states for all four metals and indeed smaller resonances can also be observed in the p and d states as well.

VI. CONCLUSIONS

In this project, plane-wave DFT calculations are used to characterize the interaction of mercury with copper, nickel, palladium, platinum, silver, and gold surfaces. Mercury binds relatively strongly to the six metal surfaces studied, with binding energies up to ~ 1 eV for Pt and Pd. The interaction with mercury in order of increased reactivity over the six metals studied is Ag < Au < Cu < Ni < Pt < Pd. With respect to the overlayers for which experimental data are available, it appears that DFT (using the PBE functional) underestimates the energy of adsorption. Binding is predicted to be stronger on the (001) faces of the metal surfaces, where mercury is situated in fourfold hollow sites as opposed to the threefold hollow sites on (111) faces. The current plane-wave DFT calculations using LDA, PW91, and LDA functionals indicate that binding at hollow sites is preferred over other high-symmetry sites, although this result is not consistent with recent relativistic cluster and embedded cluster calculations.[27] The DFT results are consistent with weak attractive and strong repulsive lateral Hg-Hg interactions, which have been posited to interpret experimental results. In general, mercury adsorption leads to decreases in the work function; adsorbate-induced work function changes are particularly dramatic on Pt. A decrease in work function is what would be expected for an electropositive adsorbate based on charge transfer from the mercury to the metal. The direction and magnitude of the calculated change in work function and the Bader charge analysis support a simple Koopmans'-theory-based interpretation of charge transfer. On Ag the net charge transfer is small, which may result from a balance between charge transfer from the mercury in to the metal and back-donation from the metal into the LUMO of the adsorbate. This is in contrast to Pt where the binding is based on very pronounced charge transfer from the mercury into the surface, resulting in a dramatic adsorbate-induced decrease in the work function.

ACKNOWLEDGMENTS

*steckel@netl.doe.gov

[1] E. B. Swain, P. M. Jakus, G. Rice, F. Lupi, P. A. Maxson, J. M. Pacyna, A. Penn, S. J. Spiegel, and M. M. Veiga, Ambio **36**, 45 (2007).

[2] R. K. Srivastava, N. Hutson, B. Martin, F. Princiotta, and J. Staudt, Environ. Sci. Technol. **40**, 1385 (2006).

[3] J. H. Pavlish, E. A. Sondreal, M. D. Mann, E. S. Olson, K. C. Galbreath, D. L. Laudal, and S. A. Benson, Fuel Process. Technol. **82**, 89 (2003).

[4] S. Ghorishi, C. Lee, W. Jozewicz, and J. Kilgroe, Environ. Eng. Sci. **22**, 221 (2005).

[5] A. A. Presto and E. J. Granite, Ind. Eng. Chem. Res. **40**, 5601 (2006).

[6] Y. Zhao, M. D. Mann, J. H. Pavlish, B. A. F. Mibeck, G. E. Dunham, and E. S. Olson, Environ. Sci. Technol. **40**, 1603 (2006).

[7] E. J. Granite, H. W. Pennline, and R. A. Hargis, Ind. Eng. Chem. Res. **39**, 1020 (2000).

[8] E. J. Granite, C. R. Myers, W. P. King, D. C. Stanko, and H. W. Pennline, Ind. Eng. Chem. Res. **45**, 4844 (2006).

[9] N. Gaston and P. Schwerdtfeger, Phys. Rev. B **74**, 024105 (2006).

[10] P. Ballone and G. Galli, Phys. Rev. B **40**, 8563 (1989).

[11] W. Y. Kim, T. Nautiyal, S. J. Youn, and K. S. Kim, Phys. Rev. B **71**, 113104 (2005).

[12] B. Paulus and K. Rosciszewski, Chem. Phys. Lett. **394**, 96 (2004).

[13] D. Andrae, U. Häussermann, M. Dolg, H. Stoll, and H. Preuss, Theor. Chim. Acta **77**, 123 (1990).

[14] W. Küchle, M. Dolg, H. Stoll, and H. Preuss, Mol. Phys. **74**, 1245 (1991).

[15] U. Häussermann, M. Dolg, H. Stoll, H. Preuss, P. Schwerdtfeger, and R. M. Pitzer, Mol. Phys. **78**, 1211 (1993).

[16] P. Schwerdtfeger, J. Li, and P. Pyykkö, Theor. Chim. Acta **87**, 313 (1994).

[17] K. A. Peterson, D. Figgen, E. Goll, H. Stoll, and M. Dolg, J. Chem. Phys. **119**, 11113 (2005).

[18] D. Figgen, G. Rauhut, M. Dolg, and H. Stoll, Chem. Phys. **311**, 227 (2005).

[19] L. J. Munro, J. K. Johnson, and K. D. Jordan, J. Chem. Phys. **114**, 5545 (2001).

[20] N. Gaston, P. Schwerdtfeger, T. Saue, and J. Greif, J. Chem. Phys. **124**, 044304 (2006).

[21] N. Gaston, B. Paulus, K. Rosciszewski, P. Schwerdtfeger, and H.

Stoll, Phys. Rev. B **74**, 094102 (2006).

[22] N. B. Balabanov and K. A. Peterson, J. Chem. Phys. **120**, 6585 (2004).

[23] N. B. Balabanov and K. A. Peterson, J. Chem. Phys. **119**, 12271 (2003).

[24] N. B. Balabanov and K. A. Peterson, J. Phys. Chem. A **107**, 7465 (2003).

[25] B. C. Shepler and K. A. Peterson, J. Phys. Chem. A **107**, 1783 (2003).

[26] P. Ballone and G. Galli, Phys. Rev. B **42**, 1112 (1990).

[27] C. Sarpe-Tudoran, B. Fricke, J. Anton, and V. Persina, J. Chem. Phys. **126**, 174702 (2007).

[28] R. G. Jones and A. W.-L. Tong, Surf. Sci. **188**, 87 (1987).

[29] P. A. Dowben, Y. J. Kime, S. Varma, M. Onellion, and J. L. Erskine, Phys. Rev. B **36**, 2519 (1987).

[30] N. P. Prince, N. K. Singh, W. Walter, D. P. Woodruff, and R. G. Jones, J. Phys.: Condens. Matter **1**, 21 (1989).

[31] N. K. Singh and R. G. Jones, Surf. Sci. **232**, 229 (1990).

[32] Y. J. Kime, J. Zhang, and P. A. Dowben, Surf. Sci. **268**, 98 (1992).

[33] N. K. Singh, P. A. D. M. A. Dale, D. Bullett, and R. G. Jones, Surf. Sci. **294**, 333 (1993).

[34] P. R. Poulsen, I. Stensgaard, and F. Besenbacher, Surf. Sci. Lett. **310**, L589 (1994).

[35] S. Soverna, R. Dressler, C. E. Düllmann, B. Eichler, R. Eichler, H. W. Gäggeler, F. Haenssler, J.-P. Niklaus, D. Piguet, Z. Qin *et al.*, Radiochim. Acta **93**, 1 (2005).

[36] P. A. Dowben, Surf. Sci. Rep. **40**, 151 (1990).

[37] P. A. Dowben, D. LaGraffe, D. Li, G. Vidali, L. Zhang, L. Dottl, and M. Onellion, Phys. Rev. B **43**, 10677 (1991).

[38] G. Kresse and J. Furthmüller, Phys. Rev. B **54**, 11169 (1996).

[39] G. Kresse and J. Furthmüller, Comput. Mater. Sci. **6**, 15 (1996).

[40] P. E. Blöchl, Phys. Rev. B **50**, 17953 (1994).

[41] G. Kresse and D. Joubert, Phys. Rev. B **59**, 1758 (1999).

[42] J. P. Perdew and A. Zunger, Phys. Rev. B **23**, 5048 (1981).

[43] D. M. Ceperley and B. J. Alder, Phys. Rev. Lett. **45**, 566 (1980).

[44] J. P. Perdew, J. A. Chevary, S. H. Vosko, K. A. Jackson, M. R. Pederson, D. J. Singh, and C. Fiolhais, Phys. Rev. B **46**, 6671 (1992).

[45] Y. Wang and J. P. Perdew, Phys. Rev. B **44**, 13298 (1991).

[46] J. P. Perdew, K. Burke, and M. Ernzerhof, Phys. Rev. Lett. **77**, 3865 (1996).

[47] M. Methfessel and A. T. Paxton, Phys. Rev. B **40**, 3616 (1989).

[48] See EPAPS Document No. E-PRBMDO-77-079807 for bulk properties, convergence information, and work function results for the bare surfaces. For more information on EPAPS, see http://www.aip.org/pubservs/epaps.html

[49] A. Migani and F. Illas, J. Phys. Chem. B **110**, 11894 (2006).

[50] E. R. Davidson, *Methods in Computational Molecular Physics* (Plenum, New York, 1983).

[51] D. M. Wood and A. Zunger, J. Phys. A **18**, 1343 (1985).

[52] P. Pulay, Chem. Phys. Lett. **73**, 393 (1980).

[53] J. Neugebauer and M. Scheffler, Phys. Rev. B **46**, 16067 (1992).

[54] G. Henkelman, A. Arnaldsson, and H. Jónsson, Comput. Mater. Sci. **36**, 254 (2006).

[55] T. C. Leung, C. L. Kao, W. S. Su, Y. J. Feng, and C. T. Chan, Phys. Rev. B **68**, 195408 (2003).

[56] M.-L. Bocquet, A. M. Rappe, and H.-L. Dai, Mol. Phys. **103**, 883 (2005).

[57] H. J. Monkhorst and J. D. Pack, Phys. Rev. B **13**, 5188 (1976).

[58] P. J. Feibelman, B. Hammer, J. K. Nörskov, F. Wagner, M. Scheffler, R. Stumpf, R. Watwe, and J. Dumesic, J. Phys. Chem. B **105**, 4018 (2001).

[59] G. Kresse, A. Gil, and P. Sautet, Phys. Rev. B **68**, 073401 (2003).

[60] R. C. van Zee, S. C. Blankespoor, and T. S. Zwier, J. Chem. Phys. **88**, 4650 (1988).

[61] T. A. Koopmans, Physica (The Hague) **1**, 104 (1933).

[62] Kenneth D. Jordan (private communication).